Article

High-Resolution Laser Spectroscopic Survey of the $H^3\Sigma_u^- - X^3\Sigma_g^-$ Electronic Transition of Si_2

Boxing Zhu, Jingwang Gu, Chunting Yu, Zengjun Xiao, Yang Chen,* and Dongfeng Zhao*

Read Online

ACCESS | 📊 Metrics & More | 📖 Article Recommendations | SI Supporting Information

ABSTRACT: Rotationally resolved spectra of the $H^3\Sigma_u^- - X^3\Sigma_g^-$ electronic transition bands of Si_2 have been experimentally studied using laser-induced fluorescence in the 380−520 nm range. Si_2 molecules are produced in a supersonically expanding planar plasma by discharging a silane/argon gas mixture. In total, 44 bands belonging to the $H^3\Sigma_u^- - X^3\Sigma_g^-$ electronic transition system of the most abundant isotopologue $^{28}Si_2$ are experimentally recorded. With a spectral resolution of ~0.04 cm^{-1}, the triplet spin-splitting structures in individual rotational transition lines are fully resolved. Detailed analyses on the high-resolution spectra have yielded an accurate determination of spectroscopic constants for both $X^3\Sigma_g^-$ and $H^3\Sigma_u^-$ states. The spin−spin interaction constants for the two triplet states are found to be comparable ($\lambda \approx 1.5$ cm^{-1}), which may originate from the 3p atomic orbital interaction in the triplet Si_2 molecule. The measured isotopologue spectra of $^{29}Si^{28}Si$ and $^{30}Si^{28}Si$ indicate that the $H^3\Sigma_u^- - X^3\Sigma_g^-$ transition system of $^{29}S^{28}S$ and $^{30}S^{28}S$ can be reasonably reproduced by the isotope mass-scaling rule. Spectroscopic parameters, including the Franck−Condon factors, the Einstein coefficients, and the oscillator strengths, are also determined from the experimental results and the Rydberg−Klein−Rees (RKR) calculations. The agreement between the experimentally measured and calculated dispersed fluorescence spectra indicates that the RKR calculations with the molecular constants determined in this work can accurately reproduce the diatomic potentials of both states. These molecular data provide a benchmark in high-level theoretical studies on Si_2 and likely other small silicon clusters.
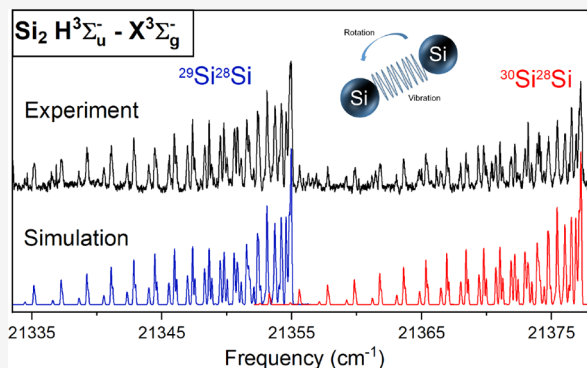
1. INTRODUCTION

Silicon is an important electronic material. Small silicon-bearing molecules are important intermediates in silicon wafer etching processes in the semiconductor industry. In astrochemistry, silicon-bearing molecules have been suggested to play a central role in the gas-phase formation of interstellar dust grains. So far, more than 10 silicon-bearing molecules, such as SiN,[1] SiC,[2] Si_2C,[3] and SiC_{2-4},[4−6] have been detected in the gas phase in the stellar atmospheres and/or circumstellar envelopes of evolved carbon stars. Many of them can participate in complex gas-phase reactions, forming the building blocks of the silicate or silicon carbide dust grains.[7] In addition to the species already detected, chemical models have also predicted more silicon-bearing molecules to be involved in the gas-phase astrochemistry, such as SiH_2, Si_2H_2, and Si_3.[8]

The disilicon molecule (Si_2) is one of the simplest silicon-bearing species. Due to the lack of a permanent dipole moment in homonuclear diatomic molecules, it cannot be detected via pure rotational and/or rotational−vibrational transitions. Similar to C_2, strong electronic transition spectra provide an alternative approach to spectroscopic observations and characterizations. Over the past decades, extensive laboratory experiments[9−16] have been performed to study the electronic

spectra and chemical reaction properties of Si_2. In 1955, Douglas observed and analyzed the $H^3\Sigma_u^- - X^3\Sigma_g^-$ and $L^3\Pi_g - D^3\Pi_u$ electronic transition bands of Si_2 in the blue and near ultraviolet (UV) regions by electric discharge.[10] Soon after, near-UV absorption spectra of the $K^3\Sigma_u^- - X^3\Sigma_g^-$ and $N^3\Sigma_u^- - X^3\Sigma_g^-$ transitions of Si_2 were recorded by Verma and Warsop in a flash photolysis experiment[11] from which the ground state of Si_2 was identified as $X^3\Sigma_g^-$. More extended studies were performed later, focusing on other electronic transition systems in wavelength regions, covering from mid-infrared to deep-UV. Meanwhile, a number of theoretical studies[15,17−19] have also been performed to calculate the complex electronic configurations and state energies, providing a theoretical support for understanding the reported experimental spectra.

Of particular interest is the $H^3\Sigma_u^- - X^3\Sigma_g^-$ transition system in the 380−450 nm range that was first reported by Douglas.[10] It

is the strongest band system in the visible region. Douglas made rotational–vibrational analyses on some well-resolved bands and suggested a large change of the rotational constant $(B'-B'')$, which reflects the change of the Si–Si bond length upon the $H^3\Sigma_u^- - X^3\Sigma_g^-$ electronic transition. Meanwhile, vibrational assignments for the $H^3\Sigma_u^- - X^3\Sigma_g^-$ system were challenging because a limited number of bands has been observed. The most reasonable vibrational assignments of the $H^3\Sigma_u^- - X^3\Sigma_g^-$ system were given by Winstead et al. based on the argument of isotope shifts of the $^{29}Si^{28}Si$ and $^{30}Si^{28}Si$ bands measured by mass-selective resonance enhanced photoionization spectroscopy.[20]

We found from previous experimental studies that the $H^3\Sigma_u^- - X^3\Sigma_g^-$ system exhibits irregular intensity distributions in vibrational hot band progressions. This may be due to the large change of the Si–Si bond length upon electronic transition that can cause an unusual dependence of the Franck–Condon factor on the vibrational quantum number. Meanwhile, individual rotational levels in both $X^3\Sigma_g^-$ and $H^3\Sigma_u^-$ states contain triplet spin-splitting due to the spin–spin interaction, which consequently complicates the rotationally resolved spectrum. Yet, the triplet fine structures in both $X^3\Sigma_g^-$ and $H^3\Sigma_u^-$ states have not been experimentally determined. Only in the study of the 180–220 nm deep-UV spectra of the $N^3\Sigma_u^- - X^3\Sigma_g^-$ and $O^3\Sigma_u^- - X^3\Sigma_g^-$ systems in ref 13 that such triplet fine structures were partially resolved. However, a quantitative determination of the triplet fine structure parameters in the $X^3\Sigma_g^-$ ground state was not available, and the authors of ref 13 made a hypothesis that the spin–spin interaction in the $X^3\Sigma_g^-$ ground state is likely quite small and negligible in the spectral analyses.[13]

More recently, Ojha et al. reinvestigated the emission spectra of Si_2 using laser ablation of a silicon rod. From the vibrational analysis of their low-resolution emission spectra, two additional electronic transition systems close to the $H^3\Sigma_u^- - X^3\Sigma_g^-$ system were suggested.[16] On the theoretical side, despite the observation that the $H^3\Sigma_u^- - X^3\Sigma_g^-$ transition has been known as the strongest optical band system, it is not predicted in the recent ab initio calculations.[19] In that study, only a $H'^3\Sigma_u^-$ state was predicted in the optical region, which has an excitation energy ($\sim16{,}242$ cm^{-1}) significantly lower than the previously reported $H^3\Sigma_u^-$ state energy. This $H'^3\Sigma_u^-$ state seems to be one of the two proposed states by Ojha et al., but it needs to be checked by high-resolution experimental studies.

In this contribution, we present a high-resolution spectroscopic survey of the $H^3\Sigma_u^- - X^3\Sigma_g^-$ transition band system of Si_2 in the 380–520 nm range recorded in a supersonic plasma jet using the laser-induced fluorescence (LIF) technique. For some strong bands, corresponding isotopologue spectra of $^{29}Si^{28}Si$ and $^{30}Si^{28}Si$ are also recorded from which an unambiguous identification of the vibrational assignments of this band system is obtained. Spectroscopic constants for both $X^3\Sigma_g^-$ and $H^3\Sigma_u^-$ states, including vibrational and rotational constants as well as the spin–spin interaction constants, are determined from the fully rotationally resolved experimental spectra. Based on the experimentally measured fluorescence lifetimes and the dispersed fluorescence spectra for individual bands, we have also interpreted a full set of spectroscopic parameters, including Franck–Condon factors, Einstein coefficients, and oscillator strengths for the $H^3\Sigma_u^- - X^3\Sigma_g^-$ transition system. The present experiment is also motivated by the experimental search for the $H'^3\Sigma_u^-$ state proposed both theoretically and experimentally,[16,19] which is found to be nondetectable in our high-resolution spectroscopic survey.

2. EXPERIMENTAL SECTION

Experiments are performed using a laser-induced fluorescence (LIF) spectrometer in combination with a supersonic slit jet plasma source. A schematic view of the setup is shown in Figure 1. Details of the setup and operation procedures have
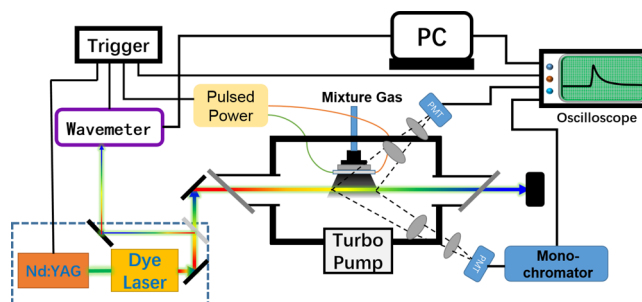
Figure 1. Schematic view of the laser-induced fluorescence setup with a supersonic slit jet expansion.

been described in our recent publication.[21] The Si_2 molecules are produced by pulsed DC discharge of a high-pressure (~6 bar) gas mixture of 0.6% SiH_4/Ar using a slit discharge nozzle. The SiH_4 sample contains silicon isotopes in their natural abundances, i.e., $^{28}Si:^{29}Si:^{30}Si \approx 1:0.05:0.03$. The slit discharge nozzle was made following the geometric design by Motylewski and Linnartz[22] and has a 0.2 mm × 30 mm slit throat. A pulsed valve (General Valve, series 9) mounted on top of the slit nozzle body controls the high-pressure gas pulse expanding into a vacuum chamber that is evacuated by a turbo molecular pump (620 l/s). High negative voltage pulses (-2000 V, 10 μs) are used to discharge the gas mixture and efficiently produce Si_2 molecules in the jet expansion.

The wavelength-tunable light source in the present work is a pulsed dye laser (Sirah, PrecisionScan) pumped by an injection-seeded Nd:YAG laser (Spectra Physics, Lab-190). For operation in the 520–430 nm wavelength range, a direct dye laser output is available by using four different coumarin dye solutions (coumarin 503, 480, 460, and 440). Meanwhile, the second-order diffraction of the grazing incidence with a 1800 l/mm grating in the dye laser oscillator is used to reduce the output laser bandwidth to less than 0.04 cm^{-1}. For the 430–380 nm tunable light, sum frequency mixing of the 700–600 nm dye laser output with the 1064 nm fundamental output of the Nd:YAG laser in a KTP crystal is employed, which provides a typical laser linewidth of ~0.04 cm^{-1}. The red output of the dye laser is obtained by using laser dye solutions of LDS722, LDS 698, DCM, R640, and R610.

The laser beam is aligned in parallel to the nozzle slit and perpendicularly crossing the gas jet at ~2 cm downstream from the nozzle. Fluorescence emission from the laser-excited molecules are collected by a telescope lens system and detected directly by a photomultiplier tube (PMT) for laser excitation spectrum measurements or by a monochromator (Zolix, Omni-λ 5007, equipped with a 1800 l/mm grating) for dispersed fluorescence spectrum measurements. An online calibration of the excitation laser frequency is realized by a wavelength meter (High Finesse, WS-7), which provides an absolute frequency accuracy better than 0.01 cm^{-1}.

Table 1. Band Positions of the $^{28}Si_2$ $H^3\Sigma_u^- - X^3\Sigma_g^-$ Transition System[a]

$v' \backslash v''$	0	1	2	3	4	5	6	7	8
0	(24,037.4)	(23,530.5)	(23,027.5)	22,528.6	22,033.7	21,542.8	21,056.0[b,c]	20,573.1 [b,c]	20,094.2[b]
1	24,312.1[b]	(23,805.1)	(23,302.1)	22,803.2	22,308.3	21,817.4[b]	21,330.6 [b,c]	20,847.7[c]	20,368.9[b]
2	24,583.0[b]	(24,076.0)	(23,573.1)	23,074.2[b]	22,579.3	22,088.4	21,601.6 [b,c]	21,118.7 [b,c]	20,639.8
3	24,850.2[b]	(24,343.2)	(23,840.3)	23,341.4	22,846.5[b]	22,355.6	21,868.8	(21,385.9)	20,907.0
4	25,113.5[b]	(24,606.5)	(24,103.6)	23,604.7	23,109.8[b]	(22,618.9)	(22,132.0)	21,649.2 [b,c]	21,170.3[b]
5	25,372.5[b]	24,865.5[b]	(24,362.6)	23,863.6[b]	23,368.7	(22,877.9)	22,391.0	21,908.1	21,429.3
6	25,628.2[b]	(25,121.2)	24,618.3[b]	24,119.4	(23,624.5)	23,133.6[b]	22,646.7	22,163.9	(21,685.0)

[a]Band intensities below the detection limit of the present experiment are enclosed in parentheses. [b]Bands whose high-resolution spectra are also recorded for detailed analysis. [c]Bands whose isotopologue spectra are also clearly recognized.
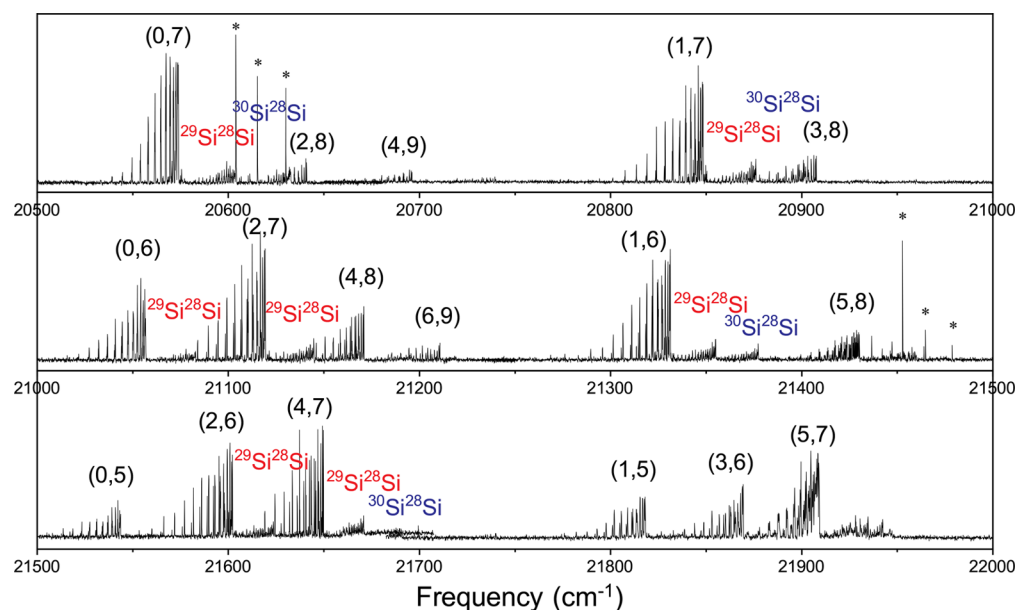
Figure 2. Part of the moderate-resolution experimental spectrum in the 455–490 nm region. Vibrational assignments (v', v'') of the $H^3\Sigma_u^- - X^3\Sigma_g^-$ transition bands of the main isotopologue $^{28}Si_2$ are labeled with black numbers, while corresponding bands of $^{29}Si^{28}Si$ and $^{30}Si^{28}Si$ are indicated by isotopologue formulas in red and blue, respectively. Discrete features marked by asterisks (*) are transition lines of SiH_2 that are also produced in the plasma.

**Table 2. Observed and Calculated Band Positions of $^{29}Si^{28}Si$ and $^{30}Si^{28}Si$**

	$^{28}Si^{28}Si$	$^{29}Si^{28}Si$		$^{30}Si^{28}Si$	
(v', v'')	observed[a]	calculated[b]	observed[c]	calculated[b]	observed[c]
(0, 7)	20,573.098	20,603.149	20,603.135	20,631.388	20,631.368
(1, 7)	20,848.351	20,876.051	20,875.995	20,902.081	20,901.506
(0, 6)	21,055.965	21,082.075	21,082.072	21,106.608	-
(2, 7)	21,118.686	21,144.092	21,144.089	21,167.966	-
(1, 6)	21,330.582	21,354.341	21,354.338	21,376.666	21,376.660
(2, 6)	21,601.553	21,623.017	21,623.001	21,643.186	-
(4, 7)	21,649.163	21,670.150	21,670.165	21,689.871	21,690.093

[a]Obtained from least square fits of the high-resolution spectra. [b]Calculated using the mass-scaling relations (eqs 6–8). [c]Obtained from least square fits of the moderate-resolution spectra of $^{29}Si^{28}Si$ and $^{30}Si^{28}Si$.

3. RESULTS AND DISCUSSION

3.1. Experimental Spectrum Survey. We have recorded the laser excitation spectra of the SiH_4/Ar plasma over the 520–380 nm range with a moderate resolution (~0.15 cm^{-1}) by scanning the dye laser wavelength with a step size of 0.002 nm. In total, 44 bands, as summarized in Table 1, are found belonging to the $H^3\Sigma_u^- - X^3\Sigma_g^-$ electronic transition system of the most abundant isotopologue $^{28}Si_2$. Fifteen of these bands have also been reported in previous studies.[10,11,20,23] As seen from the 485–455 nm part of our experimental spectra in

Figure 2, these bands exhibit well-resolved rotational structures with heavily overlapped P and R branches and no Q branches, which is indicative of a $\Sigma - \Sigma$ type of transition. In each band, the R branch turns back to the P branch side rapidly, forming a clear band head at the beginning of the R branch transition lines. This is consistent with the previous report that the $H^3\Sigma_u^-$ state rotational constant of $^{28}Si_2$ is about 30% smaller than that of the $X^3\Sigma_g^-$ ground state. The assignment of the $H^3\Sigma_u^- - X^3\Sigma_g^-$ electronic transition of these bands becomes clearly evident
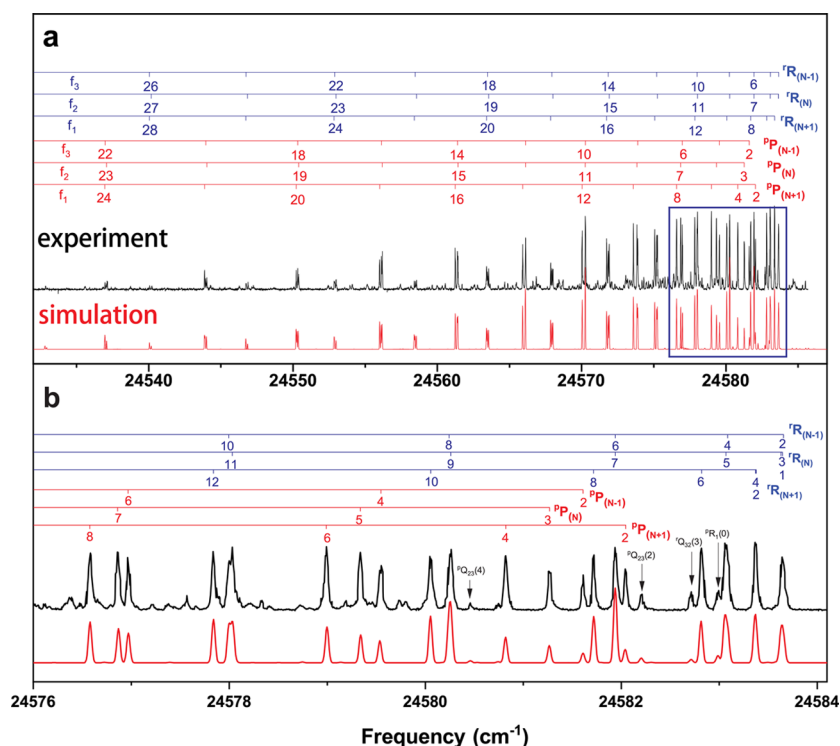
Figure 3. (a) Experimental (upper black trace) and simulated (lower red trace) high-resolution spectra of the $H^3\Sigma_u^- - X^3\Sigma_g^-$ (2, 0) band of $^{28}Si_2$. Spin-resolved rotational assignments are given by thin sticks above the experimental spectrum. A Gaussian linewidth of $\sim$0.04 cm^{-1} and a rotational temperature of $\sim$40 K are used in the spectral simulation. (b) Zoomed-in spectra in the band head region that is marked by a blue rectangle in panel (a).

from the detailed rotational analyses of individual bands, as presented in Section 3.2.

For some of the observed bands with considerable intensities, isotopologue bands of $^{29}Si^{28}Si$ and $^{30}Si^{28}Si$ are also observed, as illustrated in Figure 2. Specifically, the band at $\sim$21,060 cm^{-1} was previously assigned as the (0, 6) band by Winstead et al.[20] In their study, an examination of the isotopic shifts of the band heads was made based on mass-selective R2PI experiment. In our spectrum, the (0, 6) band of $^{29}Si^{28}Si$ is recognized at the same position ($\sim$21,080 cm^{-1}) as reported in ref 20, while the (0, 6) band of $^{30}Si^{28}Si$ is blended with the (2, 7) band of the main isotopologue of $^{28}Si_2$. For other bands such as (0, 7) and (1, 6), corresponding $^{29}Si^{28}Si$ and $^{30}Si^{28}Si$ isotopologue spectra are more clearly seen. As discussed quantitatively in Section 3.3, our high-resolution data of three isotopologues provide an unambiguous support for the corrected vibrational numbering by Winstead et al.,[20] which also makes the vibrational assignments of all 44 bands straightforward.

In Table 1, we summarize all the observed band positions and vibrational assignments. The isotopologue bands shown in Figure 2 are summarized in Table 2. It is found that many of the observed bands in our survey spectra are hot band transitions from the vibrationally excited $X^3\Sigma_g^-$ state, allowing us to assign a total of nine vibrational levels ($v'' = 0-8$) in the $X^3\Sigma_g^-$ ground state and seven vibrational levels ($v' = 0-6$) in the $H^3\Sigma_u^-$ electronically excited state. A direct recording of the (0, 0) origin band transition is unsuccessful in the present experiment. This can be explained by the very small Franck–Condon factor ($<$0.01) of the (0, 0) band transition as discussed in Section 3.4.

3.2. High-Resolution Spectra of $^{28}Si_2$. High-resolution laser excitation spectra have been recorded for 23 bands of the $H^3\Sigma_u^- - X^3\Sigma_g^-$ transition system of the main isotopologue $^{28}Si_2$ by scanning the dye laser wavelength at a speed of 0.0002 nm/s. These bands are selected to cover all the observed $X^3\Sigma_g^-$ ($v'' = 0-8$) and $H^3\Sigma_u^-$ ($v' = 0-6$) levels that are identified from the moderate-resolution survey. As an example, the high-resolution spectrum of the (2, 0) band is shown in Figure 3a. For the studied electronic transition here, both $X^3\Sigma_g^-$ and $H^3\Sigma_u^-$ states are triplet states. In such $^3\Sigma^-$ states, each rotational level with a rotational quantum number N is split into three fine spin sublevels that are defined by the total angular momentum quantum number J with $J = N + 1$ (f_1), N (f_2), and $N - 1$ (f_3), except for $N = 0$ where only $J = 1$ exists. As shown in Figure 3, the triplet fine structure of each N transition line is fully resolved. In addition, due to the centro-symmetry of the $^{28}Si_2$ molecule and the zero nuclear spin of the ^{28}Si atom, only odd-N rotational levels in the $X^3\Sigma_g^-$ ground state can be populated and accessed, as has also been depicted in Figure 3.

The rotational analysis of each high-resolution band spectrum is performed in the PGOPHER software[24] by using a standard rotational Hamiltonian for $^3\Sigma^-$ states. Individual energy levels can be expressed as

$$f_1(N + 1) = f_2(N) - 2\lambda(N + 1)/(2N - 3) + \gamma(N + 1) \tag{1}$$

$$f_2(N) = G_v + B_v N(N + 1) - DN^2(N + 1)^2 \tag{2}$$

$$f_3(N - 1) = f_2(N) - 2\lambda N/(2N - 1) - \gamma N \tag{3}$$

where G_v is the origin of the vibrational (for the ground state) or vibronic (for the $H^3\Sigma_u^-$ state) energy level, B and D are the

rotational and centrifugal distortion constants of a specific level, respectively, λ is the spin−spin interaction constant, and γ is the spin−rotation constant in a triplet electronic state. It is noted that all spin-slitting constants, λ and γ for $H^3\Sigma_u^-$ and $X^3\Sigma_g^-$, have not been determined previously. In the experimental study of the deep UV absorption spectra,[13] Lagerqvist and Malmberg observed partially resolved fine structures and suggested that the spin−spin interaction constant λ in the $X^3\Sigma_g^-$ could be comparatively small. In our high-resolution spectra, the fully resolved fine structures, specifically those in the low-N transition lines that are more significantly affected by the spin−spin interaction and, hence, better resolved, allow the determination of the $f_1(N + 1)$ and $f_3(N − 1)$ transition components and spin-resolved assignments.

Details of analyzing individual band spectra are given as follows: As the first step, preliminary fits on the combination differences of rotational levels are performed for lower and upper states separately, leading to a set of preliminary spectroscopic constants B and λ. Here, only the strong and completely unblended spectral lines are used to ensure the reliability of the fits. Fitting results at this step further provide an additional check on the assignments of weak and partially blended transitions and help to discriminate weak transition lines from nearby isotopologue bands in the experimental spectrum. A global fit is then performed to derive the accurate molecular constants with inclusion of the vibrational level energies G_ν and centrifugal distortion constants (D' and D''). It is found from the fits that inclusion of the spin−rotation interaction constant γ' for the $H^3\Sigma_u^-$ state is also needed. In contrast, the constant γ'' for the $X^3\Sigma_g^-$ ground state is negligible, i.e., the spin−rotation interaction in the $X^3\Sigma_g^-$ ground state is significantly weaker than that in the $H^3\Sigma_u^-$ state. We have also compared the spectroscopic constants obtained from the combination of different fits and the global fit. A good agreement with differences less than one standard deviation is found, indicating negligible correlations between the derived $X^3\Sigma_g^-$ and $H^3\Sigma_u^-$ constants. In the Supporting Information (Table S1), we have compiled the full list of spin-resolved transition frequencies determined from experimental spectra, their spin−rotation assignments, and the observed−calculated (o-c) deviations of the fits for all the 28 analyzed bands. The obtained spectroscopic constants for $X^3\Sigma_g^-$ ($\nu'' = 0-8$) and $H^3\Sigma_u^-$ ($\nu' = 0-6$) levels are summarized in Tables 3 and 4, respectively. A simulation of the (2, 0) band spectrum by using the determined spectroscopic constants, a Gaussian

Table 3. Spectroscopic Constants (in cm⁻¹) of the $X^3\Sigma_g^-$ Ground State of $^{28}Si_2$ [a]

ν''	$G_{\nu''}$	B''	λ''
0	0	0.23827(4)	1.401(10)
1	506.980(3)	0.23712(7)	1.419(3)
2	1009.928(3)	0.23584(7)	1.431(3)
3	1508.848(1)	0.23418(5)	1.465(19)
4	2003.7425(5)	0.23303(4)	1.517(12)
5	2494.6108(6)	0.23161(4)	1.458(15)
6	2981.479(2)	0.23045(3)	1.636(23)
7	3464.3456(9)	0.22915(7)	1.538(7)
8	3943.2059(8)	0.22742(5)	1.554(21)

[a]Numbers in the parentheses are one standard deviation in the last significant digit as obtained from the fits.

Table 4. Spectroscopic Constants (in cm⁻¹) of the $H^3\Sigma_u^-$ State of $^{28}Si_2$ [a]

ν'	$G_{\nu'}$	B'	λ'	γ'
0	24,037.444(3)	0.17175(3)	1.440(3)	−0.031(13)
1	24,312.061(1)	0.170255(8)	1.438(2)	0.00087(10)
2	24,583.032(2)	0.168973(5)	1.523(2)	0.00113(7)
3	24,850.225(1)	0.167710(5)	1.552(2)	0.00131(7)
4	25,113.509(2)	0.16647(2)	1.481(2)	0.0016(2)
5	25,372.487(2)	0.16501(2)	1.124(2)	0.0079(2)
6	25,628.202(2)	0.16379(2)	1.512(2)	0.0029(2)

[a]Numbers in the parentheses are one standard deviation in the last significant digit as obtained from the fits.

linewidth of ∼0.04 cm⁻¹, and a rotational temperature of ∼40 K, is shown in Figure 3 where a good agreement between the experimental and simulated spectrum can be seen.
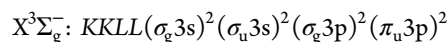
Using the spectroscopic constants, $X^3\Sigma_g^-$ and $H^3\Sigma_u^-$ state equilibrium constants can be obtained by

$$G_\nu = T_e + \omega_e\left(\nu + \frac{1}{2}\right) - \omega_e\chi_e\left(\nu + \frac{1}{2}\right)^2 \quad (4)$$
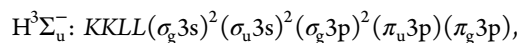
$$B_\nu = B_e - \alpha_e\left(\nu + \frac{1}{2}\right) \quad (5)$$

where T_e is the electronic term value, ω_e is the harmonic vibrational frequency, $\omega_e\chi_e$ is the anharmonic vibrational constant, B_e is the equilibrium rotational constant, and α_e is the vibration−rotation interaction constant. The result is summarized in Table 5.

In ref 13, the spin−spin interaction constants in $N^3\Sigma_u^-$ and $O^3\Sigma_u^-$ states of $^{28}Si_2$ were tentatively derived by assuming the spin-splitting in the $X^3\Sigma_g^-$ ground state to be negligible. The assumption was made based on the nonresolved triplet spin-splitting in the $H^3\Sigma_u^- - X^3\Sigma_g^-$ and $K^3\Sigma_u^- - X^3\Sigma_g^-$ transition spectra. Here, our experiment results in a spin−spin interaction constant of $\lambda'' \approx 1.5$ cm⁻¹ for $X^3\Sigma_g^-$, which is nearly one order of magnitude larger than the ground rotational constant and cannot be neglected in the analysis of the high-resolution data. In addition, we also obtain comparable values (∼1.5 cm⁻¹) of λ for the $X^3\Sigma_g^-$ and $H^3\Sigma_u^-$ states, which explains the small spin-splitting in previous low-resolution spectra. The electronic configurations for the $X^3\Sigma_g^-$ and $H^3\Sigma_u^-$ states are

$$X^3\Sigma_g^-: KKLL(\sigma_g3s)^2(\sigma_u3s)^2(\sigma_g3p)^2(\pi_u3p)^2$$

and

$$H^3\Sigma_u^-: KKLL(\sigma_g3s)^2(\sigma_u3s)^2(\sigma_g3p)^2(\pi_u3p)(\pi_g3p),$$

respectively.[25] The comparable λ values are attributed to the fact that the unpaired electrons in both states originate from the 3p atomic orbitals, which leads to very similar spin−spin interactions. Following this argument, the $K^3\Sigma_u^-$ state with an electronic configuration of $K^3\Sigma_u^-: KKLL(\sigma_g3s)^2(\sigma_u3s)^2(\sigma_g3p)(\pi_u3p)^2(\pi_g3p)$ may also have spin−spin interaction constants comparable to the $X^3\Sigma_g^-$ ground state. Indeed, the spin-splitting of the $K^3\Sigma_u^- - X^3\Sigma_g^-$ transition system is too small to be resolved in early low-resolution experimental spectra.[11] Based on the present results, the spin−spin interaction constants λ' in the $N^3\Sigma_u^-$ and $O^3\Sigma_u^-$ states suggested by Lagerqvist and Malmberg should be corrected using $\lambda'' \approx 1.5$ cm⁻¹. A high-resolution study as presented for the $H^3\Sigma_u^- - X^3\Sigma_g^-$ system here will help to more accurately determine the spin-splitting effect in the

Table 5. Equilibrium Molecular Constants (in cm^{-1}) of X$^3\Sigma_g^-$ and H$^3\Sigma_u^-$ States of ^{28}Si$_2$

molecular constants	X$^3\Sigma_g^-$		H$^3\Sigma_u^-$	
	this work[a]	refs[b]	this work[a]	refs[c]
T_e	−	−	24,153.89(8)	24,151.86
ω_e	511.026(4)	510.98	277.97(11)	279.28
$\omega_e\chi_e$	2.0085(10)	2.02	1.64(4)	1.99
$\omega_e y_e$	0.00109(8)	−	−0.034(5)	−
B_e	0.23906(10)	0.2390	0.17232(6)	0.17255
α_e	0.00134(2)	0.0013	0.00132(2)	0.00135
r_e/(Å)	2.246(1)	2.246	2.6384(6)	2.663

[a]Uncertainties (in parentheses) are 1σ in the last significant digit. [b]Ref 11. [c]Ref 20.

rotational levels of the higher lying K$^3\Sigma_u^-$, N$^3\Sigma_u^-$, and O$^3\Sigma_u^-$ states.

3.3. ^{29}Si^{28}Si and ^{30}Si^{28}Si Spectra. The spectroscopic constants obtained above are only for the main isotopologue ^{28}Si$_2$. In the present experiment, several bands belonging to the less abundant ^{29}Si^{28}Si and ^{30}Si^{28}Si are also observed in the moderate-resolution survey as shown in Figure 2. It is noted here that, since ^{29}Si^{28}Si and ^{30}Si^{28}Si are heteronuclear diatomic molecules, both odd- and even-N rotational levels in their ground states can be populated. As a consequence, individual ^{29}Si^{28}Si and ^{30}Si^{28}Si band spectra contain transition lines two times as dense as those of ^{28}Si$_2$. Although the triplet spin-splitting structures are only partially resolved in the moderate-resolution spectra, an additional check of the vibrational assignments of the whole H$^3\Sigma_u^-$−X$^3\Sigma_g^-$ transition system is still available based on the obtained spectroscopic constants for ^{28}Si$_2$ and the mass-scaling rule. Namely, the molecular constants for ^{29}Si^{28}Si and ^{30}Si^{28}Si isotopologues can be calculated using the mass-scaling relations

$$B_v^{(i)} = \rho^2 B_e - \rho^2 \alpha_e\left(v + \frac{1}{2}\right) \tag{6}$$

$$G_v^{(i)} = T_e + \rho\omega_e\left(v + \frac{1}{2}\right) - \rho^2\omega_e\chi_e\left(v + \frac{1}{2}\right)^2 \tag{7}$$

where the superscript i denotes the isotopologue molecule (^{29}Si^{28}Si or ^{30}Si^{28}Si), and the mass-scaling factor ρ is defined by the square root of the reduced mass ratio of ^{28}Si$_2$ and i

$$\rho = \sqrt{\frac{\mu}{\mu^i}} \tag{8}$$

Using the equations above, we have directly calculated the spectroscopic constants for ^{29}Si^{28}Si and ^{30}Si^{28}Si, which consequently enable the simulations of the band spectra for a direct comparison with the experimental results. In the spectral simulation, the spin−spin interaction constants are fixed to the same values as that for ^{28}Si$_2$. Figure 4 shows a comparison of the experimental and simulated (1, 6) band spectra of ^{29}Si^{28}Si (blue trace) and ^{30}Si^{28}Si (red trace). Inclusion of the spin−rotation interaction constant γ' for the H$^3\Sigma_u^-$ state is found unnecessary in the simulation of the moderate-resolution spectra. A good agreement between the experimental and simulated spectra can be seen. For a more quantitative comparison, we have also performed rotational analyses of the isotopologue bands and derived a set of spectroscopic constants. In Table 6, the two sets of the spectroscopic constants for the (1, 6) band, obtained by mass-scaling relations and by fitting the experimental spectrum, respectively, are summarized. Again, an agreement within one
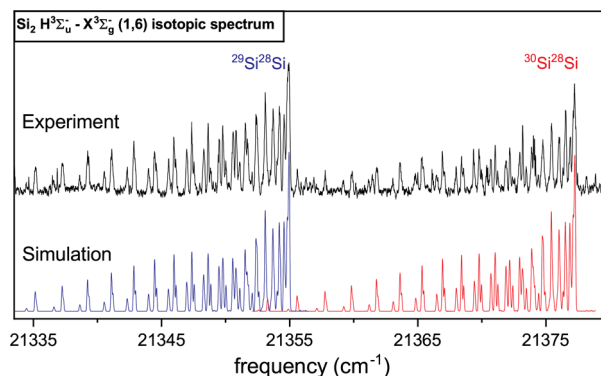
Figure 4. Experimental spectra of the H$^3\Sigma_u^-$−X$^3\Sigma_g^-$ (1, 6) bands of ^{29}Si^{28}Si and ^{30}Si^{28}Si. The simulated spectra of the two bands are shown in the lower part of the figure. A Gaussian linewidth of ∼0.15 cm^{-1} and a rotational temperature of ∼40 K are used in the spectral simulation.

standard deviation can be found between the two sets of spectroscopic constants. For all other isotopologue bands that are measurable in our spectroscopic survey, the mass-scaling rule is found to work as good as for the (1, 6) band (see a comparison of the band origin values in Table 2). Although the high-resolution isotopologue spectra are not recorded and studied in detail here, we conclude that the H$^3\Sigma_u^-$−X$^3\Sigma_g^-$ transition system of ^{29}Si^{28}Si and ^{30}Si^{28}Si can be reasonably reproduced by using the mass-scaling rule and the molecular constants of the main isotopologue ^{28}Si$_2$. In addition, the analyses of the rotationally resolved isotopologue spectra also provide a convincing argument for the vibrational assignments of the whole H$^3\Sigma_u^-$−X$^3\Sigma_g^-$ transition system.

3.4. H$^3\Sigma_u^-$ State Lifetimes, Dispersed Fluorescence Spectra, and Franck−Condon Factors. In the present experiment, Si$_2$ molecules are measured in a supersonic jet that provides a nearly collision-free environment, and the fluorescence decay is only caused by simultaneous emission of the laser-excited molecules. Thus, the radiative lifetimes of the H$^3\Sigma_u^-$ ($v' = 0-6$) levels can be determined directly from the decay time constants of the fluorescence emission by monoexponentially fitting the time-resolved fluorescence decay traces. The time-resolved fluorescence decay traces are recorded by fixing the excitation laser wavelengths at individual band heads and averaged for 200 laser shots. The residual background arising from laser scattering and discharge glow is also subtracted from each fluorescence decay trace prior to the monoexponential fit. The results are listed in Table 7.

Dispersed fluorescence spectra have also been measured to investigate the vibrational band intensities and the Franck−Condon factors of the H$^3\Sigma_u^-$−X$^3\Sigma_g^-$ transition system. This is

Table 6. Spectroscopic Constants for the (1, 6) Band Transition of $^{29}Si^{28}Si$ and $^{30}Si^{28}Si$

		$^{29}Si^{28}Si$		$^{30}Si^{28}Si$	
spectroscopic constants	$^{28}Si^{28}Si$	calculated[a]	simulation[b]	calculated[a]	simulation[b]
v''	2981.479	2954.18	2954.18	2928.53	2928.53
v'	24,312.061	24,308.53	24,308.53	24,305.21	24,305.21
B''	0.23045	0.22648	0.2267(2)	0.22277	0.2229(2)
B'	0.170255	0.16732	0.1677(2)	0.16458	0.1648(2)
λ''	1.636	1.636[c]	1.55(2)	1.636[c]	1.55(2)
λ'	1.438	1.438[c]	1.45(2)	1.438[c]	1.45(2)

[a]Calculated by mass-scaling relations. [b]Uncertainties (in parentheses) are 1σ in the last significant digit. [c]Fixed.

Table 7. Radiative Lifetimes (τ) of the $H^3\Sigma_u^-$ ($v' = 0-6$) Levels[a]

v'	τ (ns)
0	93.5(8)
1	109.9(15)
2	101.4(18)
3	106.9(13)
4	102.2(8)
5	98.4(9)
6	92.6(8)

[a]Numbers in the parentheses are three standard deviations in the last significant digit as obtained from monoexponential fits.

done by fixing the excitation laser wavelength at a selected band head and recording the wavelength-resolved fluorescence spectrum via a monochromator (see Figure 1). The dispersed fluorescence is acquired by gating the time-resolved fluorescence signal with a 300 ns time gate whose starting edge is delayed from the laser pulse by 20 ns. The 20 ns time delay is found to be helpful in removing the laser scattering signal from the fluorescence emission. Since the wavelength coverage of individual dispersed fluorescence spectra is typically larger than 300 nm, we have also calibrated the spectra by using the wavelength-dependent dispersion efficiency of the monochromator and the detector response function. As an example, Figure 5 shows the dispersed fluorescence spectrum of the $H^3\Sigma_u^-$ $v' = 0$ level recorded with the excitation of the (0, 7) band head at ~20,578.7 cm^{-1}. Individual spectral features can be immediately assigned as the (0, $v'' = 4-17$) emission band transitions based on the $X^3\Sigma_g^-$ state vibrational constants that we have determined in Table 5. It is noticed that the (0, 0) emission band is completely below our detection limit in the dispersed fluorescence spectrum, indicative of a negligible transition probability of the (0, 0) band. This is consistent with the fact that the (0, 0) band cannot be detected in the laser excitation spectrum survey even if we increase the laser pulse energy to several millijoules.

The relative band intensity $I_{v'v''}$ for the (v', v'') emission transition can be described by[26]

$$I_{v'v''} \propto \nu_{v'v''}^4 |R_{v'v''}|^2 \qquad (9)$$

where $\nu_{v'v''}$ is the (v', v'') band transition frequency (i.e., the band origin, in cm^{-1}) and $|R_{v'v''}|^2$ is the square of the overlap integral, which is also defined as the Franck–Condon factor ($q_{v'v''}$). For diatomic molecules, the Franck–Condon factors ($q_{v'v''}$) can be calculated based on the Rydberg–Klein–Rees (RKR) theory,[27] which can be used to reproduce the potential energy surfaces using the experimentally determined spectroscopic constants. We have performed the calculations following routines discussed in ref 27 and using the constants in Table 5.
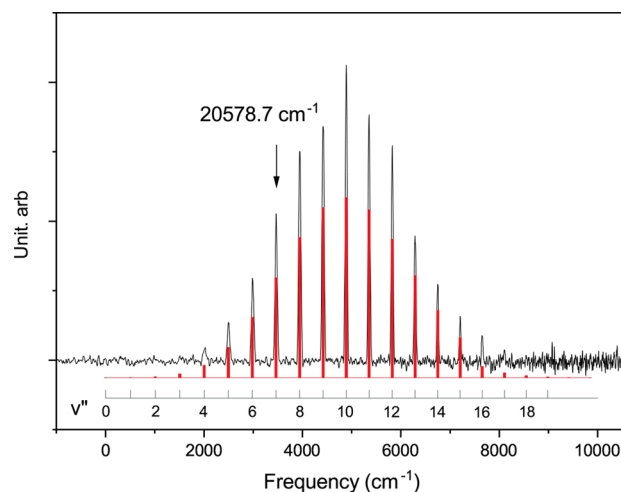

Figure 5. Dispersed fluorescence spectrum measured by fixing the excitation laser at the (0, 7) band head (20,578.7 cm^{-1}, indicated by the black arrow). The spectrum has been shifted relative to the (0, 0) band position. Transition assignments from the $H^3\Sigma_u^-$ state ($v' = 0$) to v'' vibrational levels are indicated below the spectrum. The stick spectra in red are the calculated emission spectra using the Franck–Condon factors predicted by the RKR model.

The resulting $q_{v'v''}$ are further used to interpret the dispersed fluorescence spectra. In Figure 5, the calculated stick spectrum for the (0, $v'' = 0-20$) emission bands is shown for a direct comparison to the experimental spectrum where a good agreement can be seen. For other emission bands with $v' = 1-6$, we have also made the comparisons and obtained similarly good agreement.

Using the upper state radiative lifetimes ($\tau_{v'}$) and Franck–Condon factors ($q_{v'v''}$) obtained above, the Einstein coefficient ($A_{v'v''}$), and oscillator strength ($f_{v'v''}$) for the $H^3\Sigma_u^- - X^3\Sigma_g^-$ (v', v'') transition can be subsequently calculated by[28-30]

$$A_{v'v''} = 1/\tau_{v'}\left(\frac{q_{v'v''}\nu_{v'v''}^3}{\sum_{v''} q_{v'v''}\nu_{v'v''}^3}\right) \qquad (10)$$

$$f_{v'v''} = (m_e c/8\pi^2 e^2) \times (g_1/g_2)(A_{v'v''}/\nu_{v'v''}^2) \qquad (11)$$

where m_e is the electron mass, c is the speed of light, and g_1 and g_2 are the upper and lower state degeneracies, respectively. The obtained Franck–Condon factors ($q_{v'v''}$), Einstein coefficients ($A_{v'v''}$), and oscillator strengths ($f_{v'v''}$) from the present work are summarized in the Supporting Information (Table S2). In Table 8, some selected results for $v' = 0$ are shown. It can be found from eqs 9 to 11 that the uncertainties of these values arise from the experimental measurement of $\tau_{v'}$ and the accuracy of the Franck–Condon factors ($q_{v'v''}$) calculated by

Table 8. Franck−Condon Factors ($q_{v'v''}$), Einstein Coefficients ($A_{v'v''}$), and Oscillator Strengths ($f_{v'v''}$) for the $H^3\Sigma_u^- - X^3\Sigma_g^-$ ($v' = 0$, $v'' = 0-8$) Transition Bands

$v' - v''$	λ_{vac} (Å)	λ_{air} (Å)	$q_{v'v''}$	$A_{v'v''}$ ($10^{-6} s^{-1}$)	$f_{v'v''}$ (10^3)
0 − 0	4160.176	4159.003	4.0×10^{-6}	0.00009	0.0002
0 − 1	4249.810	4248.613	5.8×10^{-5}	0.0012	0.003
0 − 2	4342.631	4341.410	4.1×10^{-4}	0.0079	0.022
0 − 3	4438.803	4437.557	0.002	0.034	0.100
0 − 4	4538.502	4537.229	0.006	0.107	0.329
0 − 5	4641.915	4640.615	0.016	0.260	0.842
0 − 6	4749.248	4747.919	0.035	0.516	1.746
0 − 7	4860.717	4859.358	0.062	0.853	3.021
0 − 8	4976.551	4975.162	0.093	1.120	4.449

the RKR model. For the used $\tau_{v'}$ values, the uncertainty mainly originates from the response time constant of the PMT detector (∼5 ns), which is significantly larger than the standard deviation of $\tau_{v'}$ in the monoexponential fits. For the $q_{v'v''}$ values, the uncertainties are difficult to be quantified, but the agreement between the calculated and experimental dispersed fluorescence indicates that the error should be small. Here, we adopt an uncertainty of ±20% for the obtained values of $q_{v'v''}$, $A_{v'v''}$, and $f_{v'v''}$, with which we are confident to account for the maximum error in the present work.

It is also possible to interpret the Franck−Condon factors ($q_{v'v''}$) from the dispersed fluorescence spectra. This is done by fitting individual emission band features with standard Gaussian functions to obtain the integral band intensities $I_{v'v''}$. Using eq 9, we have obtained a set of "experimentally determined" Franck−Condon factors. Selected $v' = 0$ and 4 results are also listed in Table 9 for a direct comparison with

Table 9. Franck−Condon Factors($q_{v'v''}$) Comparison between the Experiment and RKR Model for the $H^3\Sigma_u^- - X^3\Sigma_g^-$ ($v' = 0$, $v'' = 0-8$) and ($v' = 4$, $v'' = 0-8$) Transition Bands

$(0 - v'')$	experiment	RKR	$(4 - v'')$	experiment	RKR
0 − 0	<0.003	4.0×10^{-6}	4 − 0	0.007	0.002
0 − 1	<0.003	5.8×10^{-5}	4 − 1	0.040	0.013
0 − 2	<0.004	4.1×10^{-4}	4 − 2	0.063	0.042
0 − 3	<0.004	0.002	4 − 3	0.134	0.072
0 − 4	0.006	0.006	4 − 4	0.135	0.067
0 − 5	0.016	0.016	4 − 5	0.045	0.025
0 − 6	0.036	0.035	4 − 6	<0.0003	1.7×10^{-5}
0 − 7	0.065	0.062	4 − 7	0.037	0.025
0 − 8	0.108	0.093	4 − 8	0.083	0.052

the RKR model predicted values. We find that the experimental $q_{v'v''}$ for $v' = 0-2$ reasonably agree with the RKR predictions, showing differences typically within ±20%. However, for $v' = 3-6$, the experimental $q_{v'v''}$ are found to be somewhat larger than RKR predictions (see the $q_{4v''}$ values in Table 9 as an example). The most likely reason is that very weak emission bands that are below the detection limit of the monochromator, specifically for $v'' > 26$ bands, are not taken into account in interpretation of the absolute values of $q_{v'v''}$, which need to be normalized by $\Sigma_{v''} q_{v'v''}$. This explanation is also supported by the small Franck−Condon factors for $v'' > 26$ predicted by the RKR model (see the full data set in the Supporting Information).

3.5. Nondetection of the $H'^3\Sigma_u^-$ State. We have carefully searched for the "$H'^3\Sigma_u^- - X^3\Sigma_g^-$" transition system suggested in ref 16 where strong bands of this "$H'-X$" system were found to have comparable emission intensity to the H−X system in the 460−510 nm region in laser ablation of a silicon rod. However, the H′−X transition cannot be found in our LIF survey. By carefully comparing the present high-resolution survey to the emission data, we consider the H′−X system in ref 16 to be vibrational hot band transitions of the H−X system in the blue-green range, which were misassigned as a new optical band system due to the anomalous band intensity distributions. Limited by the spectral resolution of laser-induced plasma emission in ref 16, even the H−X band positions deviate up to several tens per centimeter from our high-resolution data, making it challenging to correct the vibrational assignments of their H−X emission bands. The determined Franck−Condon factors in this work indicate that vibrational hot bands of the H−X system in the 460−510 nm range, with $\Delta v = v' - v''$ typically in the range of −7 to −12, can have comparatively strong emission.

On the other hand, all previous theoretical calculations[15,17,19,25] predict only one $^3\Sigma_u^-$ excited state to have an excitation energy in the optical region. In early ab initio studies, this state is attributed to the $H^3\Sigma_u^-$ state with a calculated energy (∼2.85 eV) comparable to the experimentally determined $H^3\Sigma_u^-$ state energy (2.99 eV). However, in a more recent ab initio study,[19] the only $^3\Sigma_u^-$ state in the optical region, which was labeled as the $H'^3\Sigma_u^-$, is calculated to lie ∼1 eV lower than the experimentally determined $H^3\Sigma_u^-$ state. The next calculated $^3\Sigma_u^-$ in ref 19 is as high as 3.94 eV and well coincides with the $K^3\Sigma_u^-$ state in the UV spectrum.[11,23] Therefore, we conclude that the only $^3\Sigma_u^-$ excited state spectroscopically accessible from the ground state in the optical region is the $H^3\Sigma_u^-$ state studied here. The significant deviations of the recent ab initio calculations[19] from the experimentally determined $H^3\Sigma_u^-$ state energy and spectroscopic constants indicate that an accurate theoretical characterization still requires a higher level theory. In contrast, the experimentally recorded dispersed fluorescence spectra, as well as the suitability of the mass-scaling rule in the isotopologue band spectra, prove that the spectroscopic constants determined here can be used to accurately calculate $X^3\Sigma_g^-$ and $H^3\Sigma_u^-$ state potentials. This provides a benchmark for future ab initio calculations on Si_2 and likely other small silicon clusters.

4. CONCLUSIONS

The high-resolution spectroscopic survey of the $H^3\Sigma_u^- - X^3\Sigma_g^-$ electronic transition of Si_2 in the 380−520 nm range has yielded an accurate determination of spectroscopic constants for both $X^3\Sigma_g^-$ and $H^3\Sigma_u^-$ states. The spectral resolution (0.04 cm^{-1}) has enabled to fully resolve the triplet spin-splitting structures in individual rotational transition lines and, consequently, to experimentally determine the spin-splitting effect in both states for the first time. Comparable values ($\lambda \approx 1.5 \ cm^{-1}$) of the spin−spin interaction constants for both $X^3\Sigma_g^-$ and $H^3\Sigma_u^-$ states are found, which may originate from the 3p atomic orbital interaction in the triplet Si_2 molecule. A series of isotopologue band spectra of $^{29}Si^{28}Si$ and $^{30}Si^{28}Si$ have also been measured. The good agreement between the experimentally determined spectroscopic constants of the isotopologue bands and those calculated from the main isotopologue $^{28}Si_2$ indicates that the $H^3\Sigma_u^- - X^3\Sigma_g^-$ transition system of

$^{29}Si^{28}Si$ and $^{30}Si^{28}Si$ can be reasonably reproduced by the mass-scaling rule. Spectroscopic parameters for the $H^3\Sigma_u^- - X^3\Sigma_g^-$ (v', v'') transition system, including the Franck−Condon factors ($q_{v'v''}$), the Einstein coefficients ($A_{v'v''}$), and the oscillator strengths ($f_{v'v''}$) are also determined from the experimental results and the RKR calculations. The agreement between the experimentally measured and calculated dispersed fluorescence spectra indicates that the RKR calculations with the molecular constants determined in this work can accurately reproduce the potentials of both states. Like the well-known C_2 molecule, accurate molecular data for the $X^3\Sigma_g^-$ and $H^3\Sigma_u^-$ states of Si_2 are now available, providing a benchmark in future ab initio calculations on Si_2 and likely other small silicon clusters.

■ ASSOCIATED CONTENT

Ⓢ Supporting Information

The Supporting Information is available free of charge at https://pubs.acs.org/doi/10.1021/acs.jpca.0c00370.

List of the spin-resolved transition lines in the high-resolution spectra of $^{28}Si_2$ $H^3\Sigma_u^- - X^3\Sigma_g^-$, Franck−Condon factors, Einstein coefficients, and oscillator strengths for individual bands (PDF)

■ AUTHOR INFORMATION

Corresponding Authors

Yang Chen − Hefei National Laboratory for Physical Sciences at the Microscale and Department of Chemical Physics, University of Science and Technology of China, Hefei, Anhui 230026, P.R. China; Email: yangchen@ustc.edu.cn

Dongfeng Zhao − Hefei National Laboratory for Physical Sciences at the Microscale and Department of Chemical Physics, University of Science and Technology of China, Hefei, Anhui 230026, P.R. China; ⓞ orcid.org/0000-0002-8212-9435; Email: dzhao@ustc.edu.cn

Authors

Boxing Zhu − Hefei National Laboratory for Physical Sciences at the Microscale and Department of Chemical Physics, University of Science and Technology of China, Hefei, Anhui 230026, P.R. China

Jingwang Gu − Hefei National Laboratory for Physical Sciences at the Microscale and Department of Chemical Physics, University of Science and Technology of China, Hefei, Anhui 230026, P.R. China

Chunting Yu − Hefei National Laboratory for Physical Sciences at the Microscale and Department of Chemical Physics, University of Science and Technology of China, Hefei, Anhui 230026, P.R. China

Zengjun Xiao − Hefei National Laboratory for Physical Sciences at the Microscale and Department of Chemical Physics, University of Science and Technology of China, Hefei, Anhui 230026, P.R. China

Complete contact information is available at:
https://pubs.acs.org/10.1021/acs.jpca.0c00370

Notes

The authors declare no competing financial interest.

■ ACKNOWLEDGMENTS

■ REFERENCES

(1) Turner, B. E. Detection of SiN in IRC+10216. *Astrophys. J.* **1992**, *388*, L35−L38.

(2) Cernicharo, J.; Gottlieb, C. A.; Guélin, M.; Thaddeus, P.; Vrtilek, J. M. Astonomical and Laboratory Detection of the SiC Radical. *Astrophys. J.* **1989**, *341*, L25−L28.

(3) Cernicharo, J.; McCarthy, M. C.; Gottlieb, C. A.; Agúndez, M.; Velilla Prieto, L.; Baraban, J. H.; Changala, P. B.; Guélin, M.; Kahane, C.; Martin-Drumel, M. A.; et al. Discovery of SiCSi in IRC+10216: A Missing Link Between Gas and Dust Carriers of Si-C Bonds. *Astrophys. J., Lett.* **2015**, *806*, L3:1−L3:6.

(4) Thaddeus, P.; Cummins, S. E.; Linke, R. A. Identification of the SiCC Radical Toward IC+10216 - The First Molecular Ring in an Astronomical Source. *Astrophys. J.* **1984**, *283*, L45−L48.

(5) Apponi, A. J.; McCarthy, M. C.; Gottlieb, C. A.; Thaddeus, P. Astronomical Detection of Rhomboidal SiC_3. *Astrophys. J.* **1999**, *516*, L103−L106.

(6) Ohishi, M.; Kaifu, N.; Kawaguchi, K.; Murakami, A.; SAITO, S.; Yamamoto, S.; Ishikawa, S.-I.; Fujita, Y.; Shiratori, Y.; Irvine, W. M. Detection of a New Circumstellar Carbon Chain Molecule, C_4Si. *Astrophys. J. Lett.* **1989**, *345*, L83−L86.

(7) Draine, B. T. Evolution of Interstellar Dust. *Astron. Soc. Pac.* **1990**, *12*, 193−205.

(8) Tercero, B.; Vincent, L.; Cernicharo, J.; Viti, S.; Marcelino, N. A Line-Confusion Limited Millimeter Survey of Orion KL-II. Silicon-Bearing Species. *Astron. Astrophys.* **2011**, *528*, A26.

(9) Ma, Y.-j.; Li, F.-f.; Liu, J.-x.; Wang, F.-y. Imaging the Dissociation Dynamics of Si_2^+ Via Two-Photon Excitation at 193 nm. *Chin. J. Chem. Phys.* **2019**, *32*, 129−133.

(10) Douglas, A. E. The Spectrum of the Si_2 Molecule. *Can. J. Phys.* **1955**, *33*, 801−810.

(11) Verma, R. D.; Warsop, P. A. Absorption Spectrum of Si_2 Molecule. *Can. J. Phys.* **1963**, *41*, 152−160.

(12) Weltner, W., Jr.; Mcleod, D., Jr. Spectroscopy of Silicon Carbide and Silicon Vapors Trapped in Neon and Argon Matrices at 4° and 20°K. *J. Chem. Phys.* **1964**, *41*, 235−245.

(13) Lagerqvist, A.; Malmberg, C. New Absorption Systems of the Si_2 Molecule in the Vacuum Ultraviolet Region. *Phys. Scr.* **1970**, *2*, 45−49.

(14) Ho, P.; Breiland, W. G. Observation of Si_2 in a Chemical Vapor Deposition Reactor by Laser Excited Fluorescence. *Appl. Phys. Lett.* **1984**, *44*, 51−53.

(15) Sefyani, F. L.; Schamps, J. The Lowest-Lying Rydberg States of Si_2: an Ab Initio Study. *Chem. Phys.* **1995**, *191*, 155−163.

(16) Ojha, K. S.; Bajpai, P. K.; Gopal, R. Reinvestigation of Emission Spectra of Silicon Dimer in 360-540 nm Region. *J. Int. Acad. Phys. Sci.* **2011**, *15*, 105−112.

(17) Peyerimhoff, S. D.; Buenker, R. J. Potential-Energy Curves and Transition Moments for the Low-Lying Electronic States of the Si_2 Molecule. *Chem. Phys.* **1982**, *72*, 111−118.

(18) Dunlap, B. I.; Mei, W. N. Basis Set Effects on Spectroscopic Constants for C_2 and Si_2 and the Symmetry Dilemma in the $X\alpha$ Model. *J. Chem. Phys.* **1983**, *78*, 4997−5003.

(19) Shi, D.-h.; Liu, H.; Sun, J.-f.; Zhu, Z.-l.; Liu, Y.-f. Spectroscopic and Molecular Properties of 14 Selected Electronic States of Si_2 Molecule. *J. Quant. Spectrosc. Radiat. Transfer* **2011**, *112*, 2567−2583.

(20) Winstead, C. B.; Paukstis, S. J.; Gole, J. L. Spectroscopy of the $H^3\Sigma_u^-$ Electronic-State of Si_2 Using a Combined Laser Vaporization-REMPI and Oven-Based LIF Study. *J. Mol. Spectrosc.* **1995**, *173*, 311−332.

(21) Zhang, D.; Zhang, Q.; Zhu, B.; Gu, J.; Suo, B.; Chen, Y.; Zhao, D. High-Resolution Electronic Spectra of Yttrium Oxide (YO): The $D^2\Sigma^+ - X^2\Sigma^+$ Transition. *J. Chem. Phys.* **2017**, *146*, 114303.

(22) Motylewski, T.; Linnartz, H. Cavity Ring Down Spectroscopy on Radicals in a Supersonic Slit Nozzle Discharge. *Rev. Sci. Instrum.* **1999**, *70*, 1305−1312.

(23) Dubois, I.; Leclercq, H. Absorption Spectrum of Si_2 in Visible and Near-Ultraviolet Region. *Can. J. Phys.* **1971**, *49*, 3053−3054.

(24) Western, C. M. PGOPHER: A Program for Simulating Rotational, Vibrational and Electronic Spectra. *J. Quant. Spectrosc. Radiat. Transfer* **2017**, *186*, 221−242.

(25) Dixon, D. A.; Feller, D.; Peterson, K. A.; Gole, J. L. The Molecular Structure and Ionization Potential of Si_2 : The Role of the Excited States in the Photoionization of Si_2. *J. Phys. Chem. A* **2000**, *104*, 2326−2332.

(26) Herzberg, G. Molecular Spectra and Molecular Structure. Vol.1: *Spectra of Diatomic Molecules*. New York: Van Nostrand Reinhold*, 1950*, 2*nd ed.* 1951, 1.

(27) Zare, R. N. Calculation of Intensity Distribution in the Vibrational Structure of Electronic Transitions: The $B^3\Pi_0{}^+{}_u$-$X^1\Sigma_0{}^+{}_g$ Resonance Series of Molecular Iodine. *J. Chem. Phys.* **1964**, *40*, 1934−1944.

(28) De Almeida, A. A.; Singh, P. D. The OH^+ Molecule in Interstellar Clouds Absolute Oscillator Strengths and Equivalent-Widths for OH^+ ($A^3\Pi_i$-$X^3\Sigma^-$) Bands. *Astron. Astrophys.* **1981**, *95*, 383−385.

(29) Mulliken, R. S. Intensities of Electronic Transitions in Molecular Spectra I. Introduction. *J. Chem. Phys.* **1939**, *7*, 14−20.

(30) Jeunehomme, M. Oscillator Strengths of the Negative Systems of Oxygen. *J. Chem. Phys.* **1966**, *44*, 4253−4258.